Neutronics assessment of EU DEMO alternative divertor configurations

A. Valentine [*,a], N. Fonnesu [b], B. Bieńkowska [c], E. Łaszyńska [c], D. Flammini [b], R. Villari [b], G. Mariano [b], T. Eade [a], T. Berry [a], L. Packer [a]

[a] Culham Centre for Fusion Energy, Culham Science Centre, Abingdon, OX14 3DB, Oxford, UK
[b] ENEA, Department of Fusion and Nuclear Safety Technology, I-00044 Frascati Rome, Italy
[c] Institute of Plasma Physics and Laser Microfusion, ul. Hery 23, 01-497 Warsaw, Poland

ARTICLE INFO

ABSTRACT

As a demonstration fusion power plant, EU DEMO has to prove the maturity of fusion technology and its viability for electricity production. The central requirements for DEMO rest on its capability to generate significant net electric power to the grid (300 MW to 500 MW) safely and consistently. Plant availability and lifetime will approach that of a commercial fusion power plant. Operating at such regimes presents many complex challenges, of which one is plasma exhaust. To mitigate the risk that the implementation in preceding experimental devices, namely ITER, does not extrapolate to the requirement of DEMO, alternative solutions must be sought. The investigation of alternative divertor configurations was born out of this motive, seeking to resolve a 'critical' challenge for the realisation of DEMO. In this paper, we study the neutronics performance of three concepts: Single Null (SN), Super-X (SX) and X-divertor (XD). This is the first time a preliminary analysis of alternative configurations to the SN baseline has been performed. The shielding proposals and design recommendations presented herein should be integrated with other engineering and physics constraints in future iterations of the chosen divertor concept.

1. Introduction

The EU DEMO demonstration fusion power plant aims to produce 300–500 MW electricity to the grid and operate at timescales approaching that of a commercial fusion power plant. This unprecedented operating regime far exceeds what will have been achieved with ITER which, when fully commissioned, will be the worlds most powerful nuclear fusion reactor [1]. DEMO presents a range of complex challenges, many intricately interdependent based on the physics and engineering constraints of the machine. The understanding born out of operating ITER will provide a fundamental basis for solving many of these issues. However, others will necessitate pioneering research that explore novel ideas beyond ITER. The divertor is one such example where a simple extrapolation of the ITER design is potentially not viable, and alternative solutions to the problem of plasma exhaust must be sought. Indeed, in the first gate review it has been recognised that plasma exhaust is one of four 'critical' challenges for the realisation of DEMO [2].

The investigation of alternative divertor configurations (ADC) is a dedicated pathway to finding this solution through analysing the physics

and engineering viability of various divertor configurations for implementation in DEMO. In this work, we consider three such configurations, the Single Null (SN), Super-X (SX) and X-divertor (XD) [3]. This is a first time that a dedicated neutronics assessment has been performed for these concepts in a DEMO-sized machine. As such we evaluate a number of nuclear responses using 3D neutronics models, namely: neutron flux, nuclear heating, displacements per atom (DPA) and helium production. Although absolute nuclear responses are presented, this is a preliminary analysis with focus on the *comparative* performance of each concept. As such, emphasis is made on a standardised and consistent approach being adopted for all models.

In DEMO, high energy neutrons born from deuterium-tritium reactions in the plasma escape and then interact with the surrounding components of the reactor. The total neutron budget is anticipated to be as high as 10^{29} neutrons at the end of its life. Neutron interactions give rise to displacements of atoms and material transmutation which affect the overall structural integrity of components. Furthermore, nuclear reactions and scattering interactions within materials give additional heating to components which must be critically cooled in order to operate in a superconducting regime. As such, characterisation of the

---

* Corresponding author.
  E-mail address: alex.valentine@ukaea.uk (A. Valentine).

radiation fields is a critical design driver for the divertor and tokamak as a whole with impact on the lifetime, operability and maintainability of DEMO.

This paper outlines the results of the aforementioned nuclear responses with reference to specified operational limits where available. This gives a first comparative assessment from which a series of shielding and design recommendations are formulated. It is not the purpose of this paper to recommend a certain exhaust solution. Certainly, the models require a much greater level of maturity than used here. The authors instead stress that the optimal divertor solution for DEMO is to be derived via an integrated pathway including other engineering and physics disciplines. Neutronics analysis is an imperative input to this at every iteration of the design.

2. Divertor configurations

The three divertor configurations studied (Fig. 1) include homogenised representations of the primary divertor components: three distinct plasma facing layers representing the inner and outer vertical targets, the cassette body, the shielding liner and a single tungsten plasma facing layer on the shielding liner. The SN model is the baseline for current DEMO analysis [4]. XD has a large poloidal flux expansion close to the target giving an increased connection length. SX is characterised by a longer outer divertor leg, maximising the toroidal flux expansion. The shielding capability is extremely sensitive to the subtleties of the geometry as we demonstrate in this paper.

The tokamak models, unique for each configuration, are built through a process of optimisation. This is driven in the first instance by plasma physics which determines the positioning of the blanket/first wall and the toroidal field (TF) coils. The poloidal field coils are then positioned to optimise plasma performance. Further detail on the build of the reactor models can be found in [5].

3. Nuclear analysis methodology

The nuclear analysis has been performed using MCNP v6.1 [6] and MCNP v6.2 [7]. An independent MCNP model was prepared for each of the configurations including a description of all major components up the bioshield. The models were simplified to retain only bodies important to neutron-photon transport and converted into MCNP constructive solid geometry (CSG) representation using SuperMC [8]. Each of the three models were then debugged to ensure the integrity of the geometry and to validate the conservation of volumes in the conversion process.
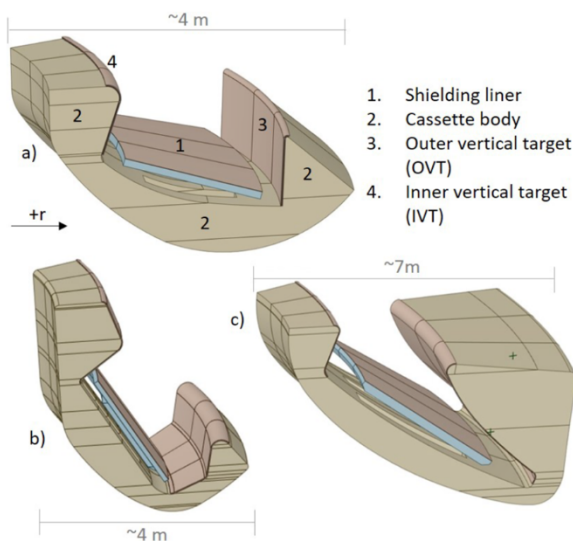

Fig. 1. Geometry of the SN (a), XD (b) and SX (c) divertors used in this analysis. The inner and outer vertical targets have three plasma facing layers.

A weight window has been produced for each of the three models using ADVANTG [9] in the global variance reduction (GVR) scheme. All nuclear responses have been computed using these weight windows. Multiple simulations were performed for each configuration owing to the number and high memory requirements of responses. These were run on the UKAEA and ENEA Cresco high performance computing clusters hosted at their respective institutions, as well as the Świerk Computing Center (CIŚ) located at the National Center for Nuclear Research (NCBJ). Some calculations were also performed using the Marconi supercomputer. All simulations have been run with 10^9 neutron histories and results normalised to a plasma neutron source intensity of 7.094×10^{20} n s^{-1}, based on 1998 MW fusion plasma source.

The nuclear data library, JEFF3.3 [10] has been used for neutron transport and the library, MCPLIB84 [11], for photon transport. The plasma source term is based on a parametric representation. The SN, XD and SX have the same major radius, aspect ratio, elongation and plasma current parameters therefore these have been taken from the SN baseline. The neutron emission profile has been validated to be equivalent for each configuration.

We have evaluated nuclear responses with the aim of demonstrating the global (across all reactor components) effect of the different divertor configurations. The entire tokamak build is significantly different in each configuration therefore it is important that the study is not solely focused on the response local to the divertor. They are also designed to give a comparative assessment to existing analysis which to date has been undertaken solely with the SN concept. The nuclear responses include: neutron flux, nuclear heating, DPA and He production. The responses have been computed using a combination of cell and mesh-based tallies. The statistical relative errors are all below 10% unless otherwise stated. For cell tallies, the 10 statistical tests presented by MCNP were also examined to ensure results are adequately converged.

4. Model description

The detailed material allocation for all components is given in

Table 1

Material description and density for the ADC MCNP models. % compositions are by volume and densities are atomic (atoms barn^{-1} cm $-$ 1). KALOS refers to Karlsruhe Lithium Orthosilicate.

Component	Material	Density
Divertor cassette body	54% Eurofer + 46% H$_2$O	8.85E-02
Shielding liner body	53% Eurofer + 47% H$_2$O	8.83E-02
Shielding liner layer I	W	6.24E-02
IVT/OVT layer I	W	6.24E-02
IVT/OVT layer II	16% CuCrZr + 39% W + 28% H$_2$O + 16% Void	6.45E-02
IVT/OVT layer III	W	6.24E-02
Blanket first wall	W	6.24E-02
Blanket front/side plates	61% Eurofer + 39% Void	5.16E-02
Blanket breeder zone	20% Eurofer + 39%Be$_{12}$Ti + 9% KALOS +31% void	7.37E-02
Blanket backplate	Eurofer	8.51E-02
VV shell + Ports	SS316LN-IG	8.59E-02
VV body	60% SS316LN + 40% H$_2$O	8.61E-02
Central solenoid	43% SS316LN + 18% r-epoxy +17% He + 12% Cu + 7% Bronze + 3% Nb$_3$Sn + 0.1% Void	7.19E-02
TF casing	SS316LN-IG	8.59E-02
TF/PF winding	As central solenoid	7.19E-02
Cryostat	SS316LN-IG	8.59E-02
Bioshield	Concrete	6.97E-02

Table 1. The materials are consistent between the different divertor concepts in this preliminary analysis and based on the DEMO Helium Cooled Pebble Bed (HCPB) concept [12,13]. The breeder zone, manifold and back support structure have been homogenised based on the volume fractions in the XD model. The different compositions of the inboard and outboard blanket modules have also been homogenised.

The SN MCNP model is shown by example in Fig. 2, with the major components that have been tallied and referred to in this paper indicated. A 22.5° representative sector is used with reflecting boundary conditions to approximate the toroidal symmetry of the tokamak.

5. Results

5.1. Neutron flux

The neutron flux for each configuration is shown in Fig. 3. This is calculated in $10 \times 10 \times 10$ cm^3 mesh voxels. In the ex-vessel region, there are clear differences between each configuration in this analysis whereby, unrealistically but nevertheless, consistently, all ports are completely open. Around the upper and lower port, the ex-vessel flux is highest in the SN, followed by the SX and then the XD. This can be explained from the relative port dimensions which are, SN (400 cm × 350 cm), SX (397 cm × 330 cm) and XD (350 cm × 280 cm). The port dimensions in the models used within this analysis were primarily driven by space constraints stemming from the positioning of the coil systems. A future, more complete analysis, should factor in all aspects driving the port dimensions such as cooling networks, heating and current drive systems, and remote maintenance needs.

The ex-vessel neutron flux around the lower port is most sensitive to the configuration of the divertor. The highest level of shielding in the divertor region is provided by the SX configuration, with the flux in the lower port opening being ∼2 orders of magnitude lower than the other two concepts. The cassette below the outer vertical target is significantly larger in volume in the SX and is positioned in the lower port aperture.

One important observation is the streaming apparent through the gap between the blanket and the divertor. A higher resolution flux map around the divertor region for the SN and XD is shown in Fig. 4. This is most prominent in the XD model where the gap is as large as 8.0 cm. The SN model similarly has a gap equal to 3.6 cm. The neutron flux field in the lower port is ∼5 × 10^{11} n cm^{-2} s^{-1} rising by an order of magnitude in line of sight of the gap, dominated by the streaming channel coupled

with the lower level of shielding provided by the outer part of the cassette relative to the other concepts. For the XD concept, bulk transport through the divertor cassette body is evident. In general, the engineering solution to gaps is the implementation of a dog leg and/or shielding inserts assuming that the penetration is an absolutely necessary design detail.

In all configurations, the streaming through the pumping port is apparent. In the XD concept, the shielding liner provides slightly better shielding than the other configurations with the resulting nuclear heat density and DPA on the vacuum vessel (VV) shell lower as a result (see Sections 5.2 and 5.4).

The position of the pumping opening with respect to the lower port opening is significant. In the SN model, the pumping opening is partly aligned with the lower port aperture which is the reason for the highest flux field in the lower port for this configuration. The opening can be considered 'better' positioned with respect to the lower port in the case of the XD and SX. However, there are nuclear limits on the heating and damage to the VV which is directly behind the opening, with shielding provided only by the divertor shielding liner. The pumping opening is the largest for the SX model however this does not offer much benefit as it just means the response is distributed over a larger area as opposed to introducing higher localized peaking, which is of most concern considering the response limits.

In the SN model, two reflector plates have been included in the space between the shielding liner and the divertor cassette for limiting thermal, alpha particles and other impurities [4]. Furthermore, a more massive shielding liner and additional neutron shielding plates included in the pumping duct area are designed to further reduce heat loads on the VV. These are not present in the simplified neutronics model of SN and it is evident that these should also be included for the alternative divertor configurations.

It is possible that the size of the pumping port can be reduced if a greater number of pumping ports around the tokamak can be introduced. The impact again depends on the position of the pumping port opening with respect to the lower port. Reducing the pumping opening in SN model would be beneficial to reducing the nuclear response local to that port. However, this would need to be weighted against the impact of having more such ports requiring further analysis.
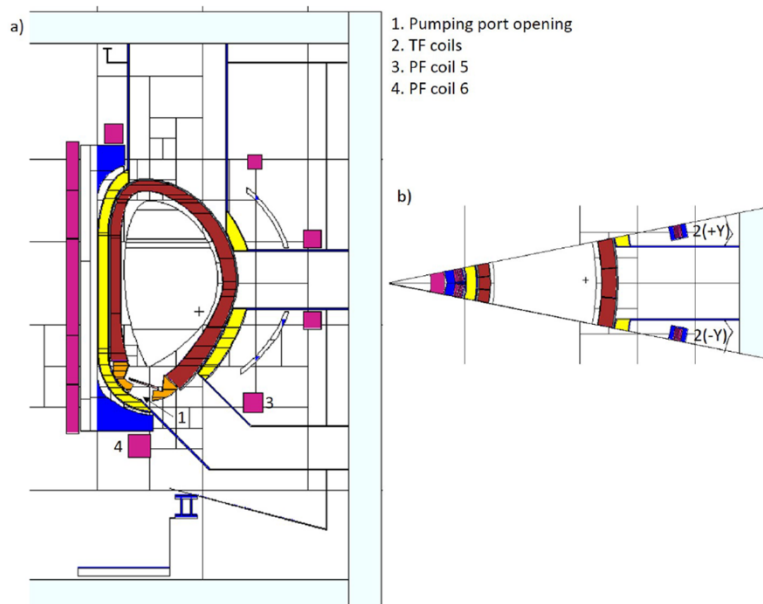
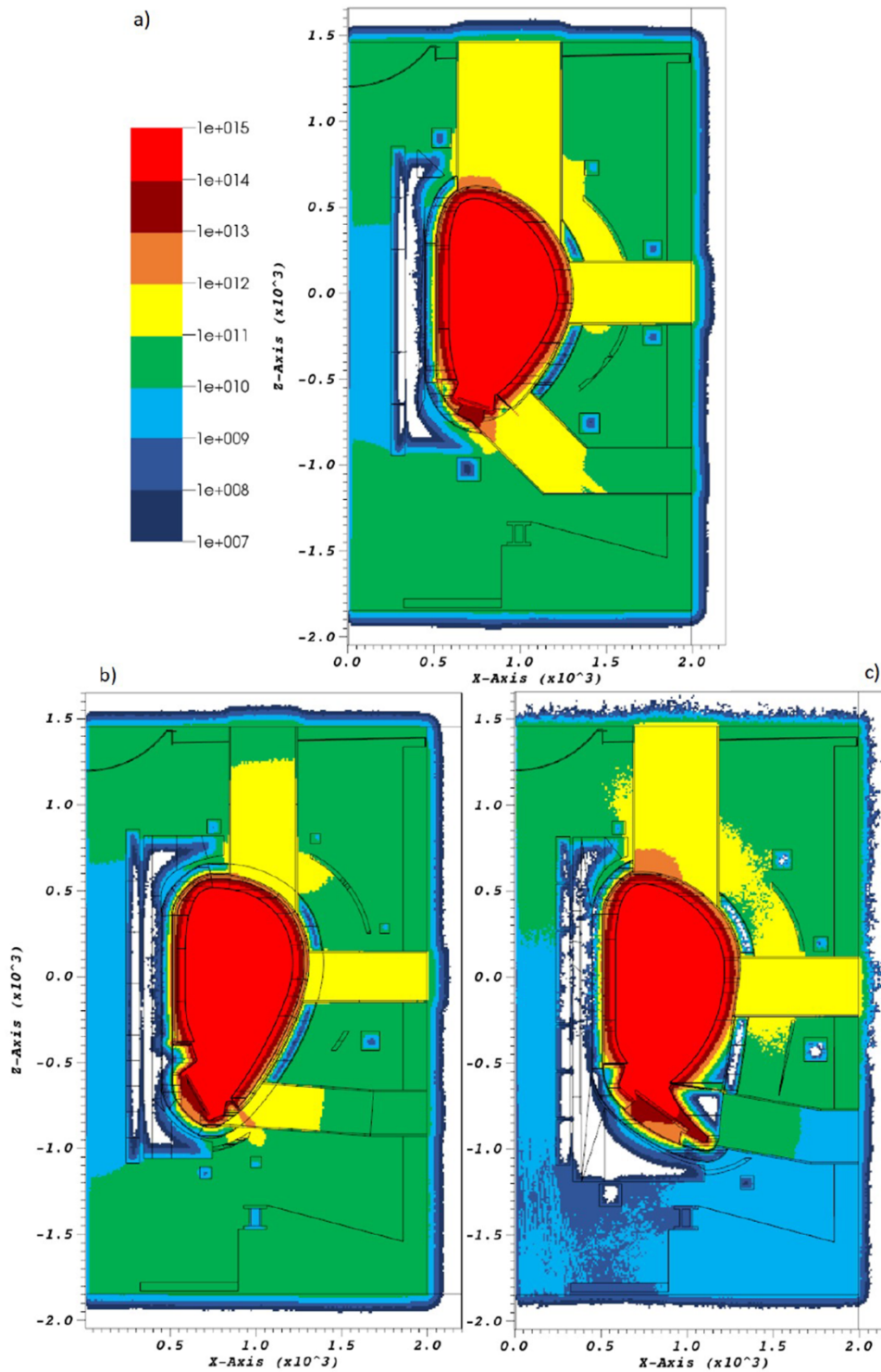**Fig. 2.** MCNP geometry of the SN model for a (a) vertical (Y=0) and (b) horizontal (Z=0) slice.

Fig. 3. Neutron flux ($n\,cm^{-2}\,s^{-1}$) in the (a) SN, (b) XD and (c) SX at Y=0. The minimum neutron flux threshold is set to 1×10^7.

5.2. Divertor and VV nuclear heating

As shown in Fig. 5, the nuclear heat density in each configuration is strongly correlated to the profile in the neutron flux within materials.

The stated target on nuclear heating in the vacuum vessel is 0.3-0.5 W cm^{-3} [14]. The neutron flux shielding weaknesses in the SN are highlighted by the highest nuclear heating observed in the vacuum vessel particularly below the pumping opening. In this region, compared to the other configurations, the nuclear heating contour at 0.1 W cm^{-3}

spans the furthest into the vacuum vessel. As a result, only for the SN is 0.3 W cm^{-3} exceeded, with peak value equal to 0.33 W cm^{-3}. This does however lie within the bounds of the target nuclear heat density.

For the XD concept the peak value in the VV is 0.05 W cm^{-3}, and for the SX, 0.09 W cm^{-3}. Localized peaking is observed on the vacuum vessel between the blanket and the divertor. Although this is in all cases below 0.3 W cm^{-3}, it is once more stressed that such streaming channels need to be avoided where possible and an integrated engineering solution is formulated together with the blanket modules. Although the
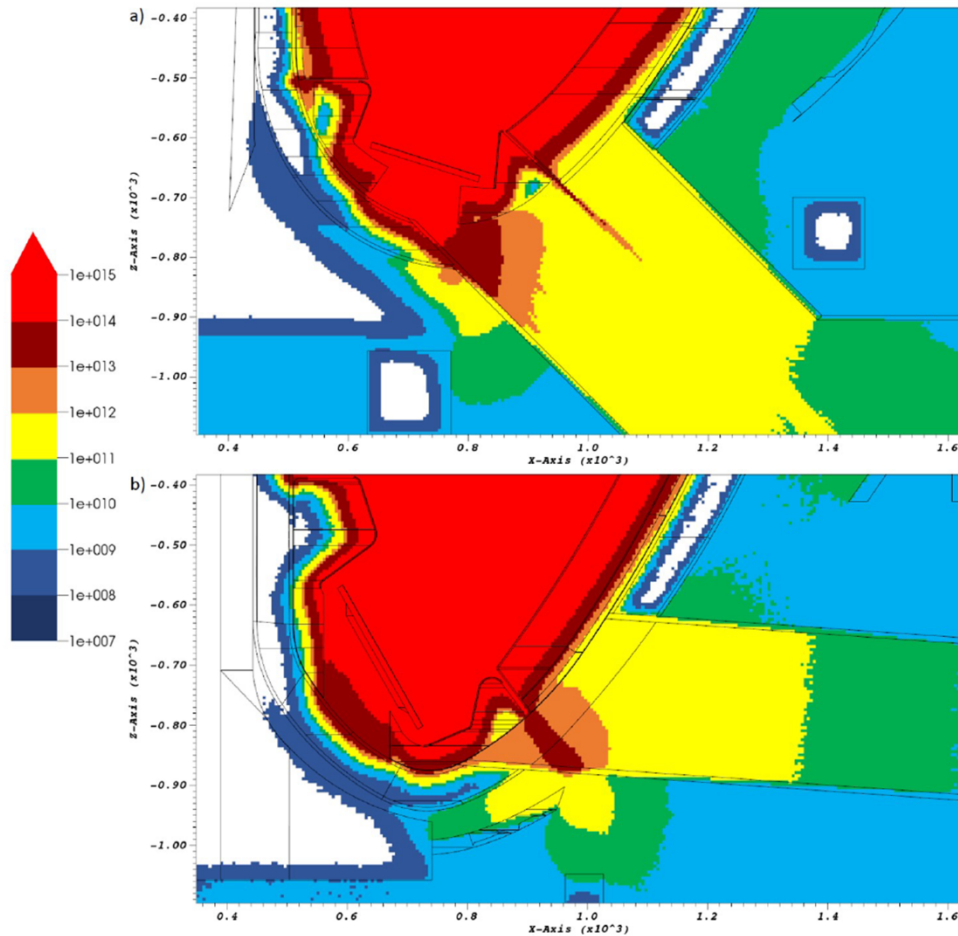
Fig. 4. Neutron flux ($n\,cm^{-2}\,s^{-1}$) local to the divertor for the (a) SN and (b) XD models at Y=0. The minimum neutron flux threshold is set to 1×10^7.

pumping opening is smaller in the XD relative to the SX, it can be seen in Fig. 5 that the heat density in the VV shell, in the outboard, extending to the walls of the lower port, is larger. It is apparent that bulk neutron transport through the cassette itself is more prevalent in this particular region of the outer vertical target.

5.3. TF coil nuclear heating

The level of shielding and design aspects highlighted in relation to the nuclear performance discussed above have a telling impact on components beyond the divertor. The nuclear heat density in the TF coils is a critical quantity that must satisfy the limit of 5×10^{-5} W cm^{-3} [14]. The TF coils in DEMO will be superconducting, cooled using liquid helium to temperatures of 4 K - maintaining these temperatures is critical to their operation. The additional heating from nuclear reactions should be limited to ensure that across the entire poloidal extent of the coil structures, the criterion for the nuclear heat density is satisfied.

The calculated poloidal profile of the nuclear heat density in the TF coils is shown in Fig. 6 for the +Y coil in the MCNP model. The lower port shielding in the SX configuration gives lower heat density in the coil for segments 3–7. Around the equatorial region, the XD model performs the best owing to the small port dimensions, which also holds true at the upper port level. The design limit is also indicated in Fig. 6 showing that for all inboard poloidal segments, the configurations are below the limit. The large differences observed in segments 3,4 and 5 are directly attributable to the different shapes of the divertor. For all outboard segments the limit is exceeded with one exception, the poloidal segments next to the lower port in the SX. Further, the effect of the streaming gap between the blanket and the divertor in the SN and XD

models is prominent in giving localised peaking poloidal segment 6 in direct line of sight of the penetration. This is the only segment where the heating in XD is higher than the SN and this is because the opening is 5 cm larger.

The open port configurations are unrealistic and have a significant impact on the ex-vessel responses. For a more detailed model, with appropriate port fillers, the TF coil heating would be reduced. Nonetheless, an increased level of shielding may still be required in the outboard region. Increased port wall thickness at lower, equatorial and upper port levels is one option. This is a potentially viable solution, though requires more detailed analysis, if the space inside the ports themselves is not available for additional shielding.

5.4. DPA

As well as limiting the nuclear heating to the TF coils, the structural integrity of the divertor must be demonstrated to ensure expected operation over anticipated lifetime. One such limiting quantity is the displacements per atom (DPA) which is an atomic based assessment of the structural damage to a material under neutron irradiation. The DPA is formulated based on the modified Kinchin-Pease method of Norgett, Robinson, and Torrens [15] ('NRT' method) whereby the neutron flux is convoluted with the NRT dpa cross section:

$$\frac{DPA}{FPY} = \frac{0.8 * 10^6 * flux}{2E_d} * n\,s^{-1} * 10^{-24} * 31558464 \qquad (1)$$

where E_d is the atomic displacement energy assumed to equal 40 eV for Eurofer. Further detail on this methodology can be found in [16]. The
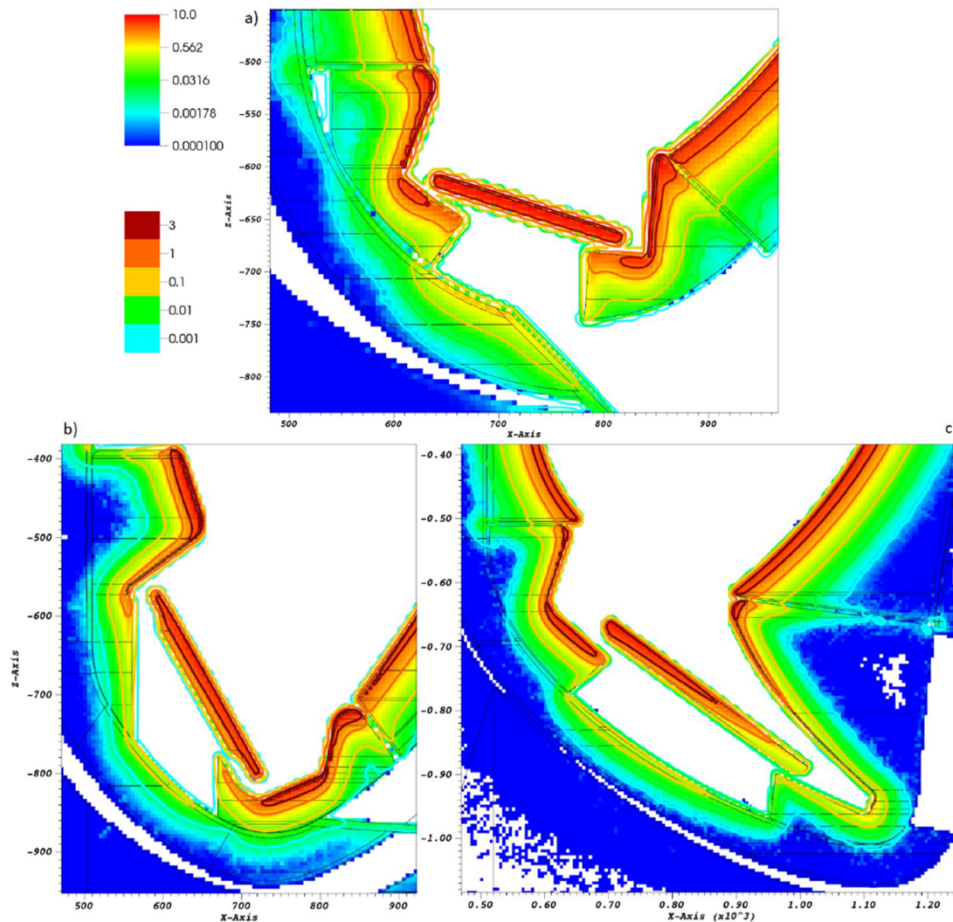
Fig. 5. Nuclear heat density (W cm^{-3}) for the (a) SN (b) XD and (c) SX configurations at Y=0.

DPA/FPY calculated in Eurofer is shown in Fig. 7.

The damage limit to the divertor in Eurofer is 6 DPA over 1.5 FPY (i. e. the target lifetime of one cassette), therefore we can assume a limit on the divertor of 4 DPA/FPY in Fig. 7. In each case, the highest DPA values are recorded on the shielding liner and on the part of the cassette below the two vertical targets which sit almost below the shielding liner. To summarise, the peak recorded values are presented in Table 2.

The limit is exceeded only in the shielding liner of the SN while the other values are close to this limit.

The shielding liner of the SX shows a distribution in DPA, with the highest DPA values observed at the exposed inboard side. The lowest values are observed at the outboard side where the shielding liner is shielded by the blanket. In contrast the peak values occur almost in the centre of the XD shielding liner because of the shielding over the upper part of the vertical targets. The distribution in DPA/FPY is fairly uniform across the shielding liner of the SN.

The high DPA/FPY in Eurofer on the cassette is caused by the absence of any plasma facing layers in the regions highlighted. Of the three configurations, the shielding liner of the XD provides the most effective shielding of these exposed regions, with almost all of the cassette body without plasma facing layers in its shadow. For both the SX and the SN, these regions of the cassette are directly exposed to the plasma.

Although the limit is exceeded only in the shielding liner of the SX, there can be large variation in DPA values and we can postulate that this limit is exceeded given the uncertainties in this preliminary analyses. A large deviation in DPA values is observed with different nuclear data libraries as demonstrated in [17], as well as the underlying uncertainty owing to the maturity of the design and modelling approximations. At the limit, the lifetimes of these cassette components is limited, with

calculations suggesting a FPY replacement frequency using the DPA/FPY limit.

The limit to DPA in stainless steel is equal to 2.75 over 6 FPY. This limit is applicable to the inner shell of the vacuum vessel, comprised of this material. In all cases, the DPA over 6 FPY was calculated to satisfy the criterion with a peak value of 2.38 DPA over 6 FPY observed in the SN concept. The peak value in the XD model below the pumping opening is 0.35 DPA over 6 FPY, and for the SX is 0.66 DPA over 6 FPY. Here, as with the results presented for the DPA/FPY in Eurofer, the need to reduce neutron streaming through the pumping opening is exemplified. It is recommended that shielding is considered above the exposed regions of the cassette body directly adjacent to the pumping port in all configurations. This could be in the form of a reflector plate foreseen in the present reference design of SN divertor [4] but not included in the simplified neutronics model.

5.5. Other nuclear responses

Helium production

The helium production has also been computed assuming Eurofer material composition. Helium production is an issue because of its migration within a material to grain boundaries leading to the onset of embrittlement. He production may also compromise the re-weldability of pipes therefore a limit of 1 appm accumulated over the lifetime of the machine is used as a criteria where such operations are required. A limit is applied to the lifetime as pipes can not be replaced and must survive the entirety of plant operations. In Fig. 8 a contour is plotted at 0.16 appm/FPY (corresponding to the 1 appm limit over 6 FPY DEMO lifetime); should re-welding be required, it can only take place beyond
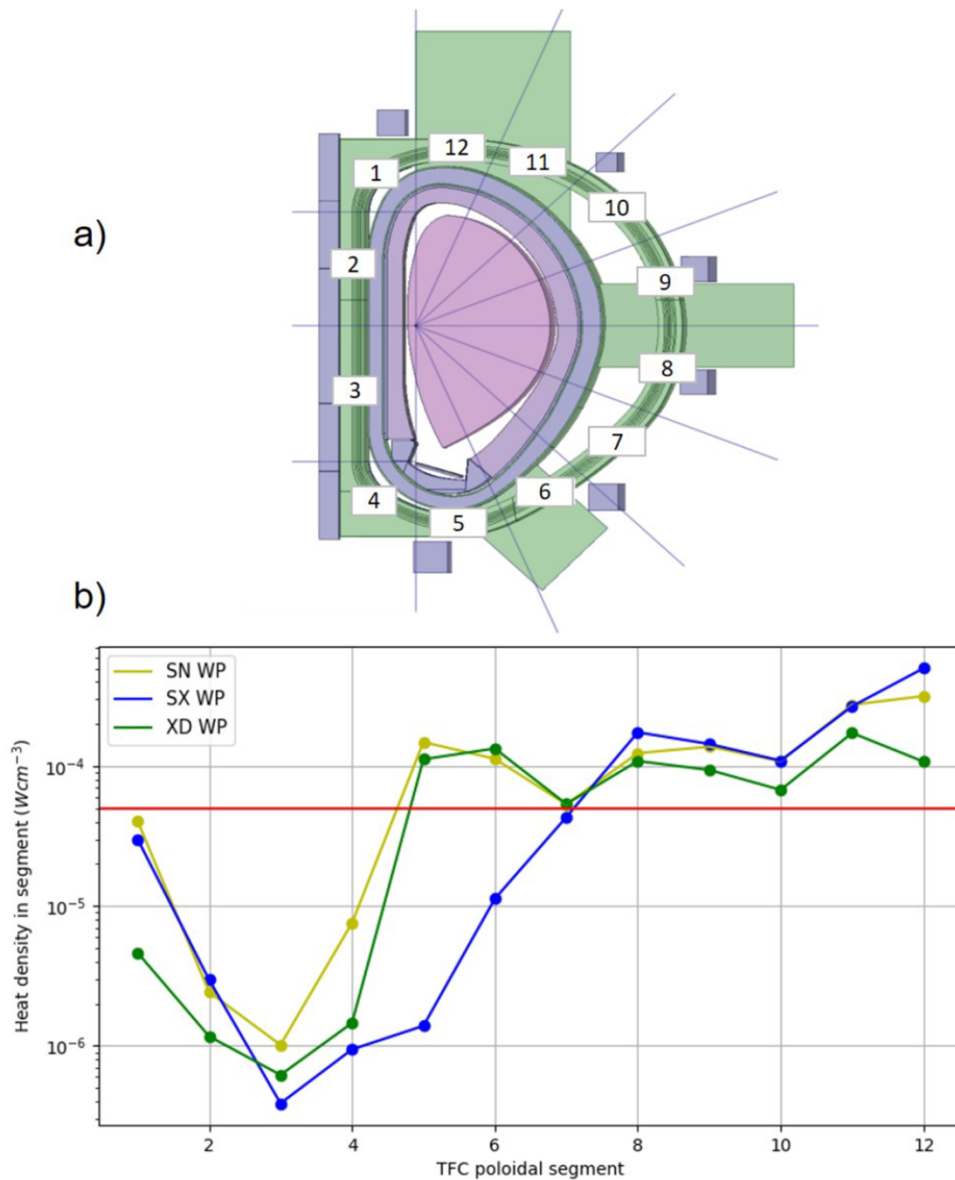
Fig. 6. (a) Poloidal TFC segment profile for the SN, SX and XD divertor concepts and (b) nuclear heat density poloidal profile in the TF coil winding pack (WP) for each configuration. The red line gives the nuclear heat density limit of 5×10^{-5} W cm^{-3}. (For interpretation of the references to colour in this figure legend, the reader is referred to the web version of this article.)

this contour.**PF coil nuclear heating**

Poloidal field (PF) coils are a critical component to machine operations that require adequate shielding to limit the nuclear heating. Table 3 gives an estimate for the integrated power load for the 360° toroidal extent of lower PF coils 5 and 6.

The relative magnitude of the power load in each case is in line with the volumes of the coils. The greatest heating in both of the lower PF coils is observed for the SN configuration. In the SN configuration these coils are either side of the lower port opening, so the increased coil heating can be attributed to the higher neutron flux in this port (Fig. 3) and the close proximity of the coils to the port walls. In the case of the XD, both PF coils 5 and 6 are positioned *below* the lower port - for this configuration PF coils 4 and 5 neighbour the port. It is an important consideration that the specific coils that are subject to the high heat loads due to the lower port opening is divertor configuration dependent. As indirectly articulated throughout this paper, this serves as demonstration of the need to integrate the analysis of nuclear responses with other engineering constraints for the reactor.

6. Conclusion

A first comparative analysis of three alternative divertor configurations that are being considered for implementation in EU DEMO has been performed. A simplified EU DEMO MCNP model with homogenized material descriptions has been produced integrating the SN, SX and the XD divertor models. Simulations have been performed to assess the relative nuclear performance of each configuration. The main conclusions that can be drawn from this work are:

- The nuclear response of the systems and materials in the ex-vessel region is strongly coupled to the size of the port openings. Future detailed conceptual models need to include the most prominent drivers for the port dimensions such as remote maintenance and pumping requirements.
- The highest neutron flux in the lower port was calculated in the SN model. This is a direct consequence of the pumping port which, unlike the other configurations, is partially aligned with the lower port aperture. A large neutron flux field in the lower port is also
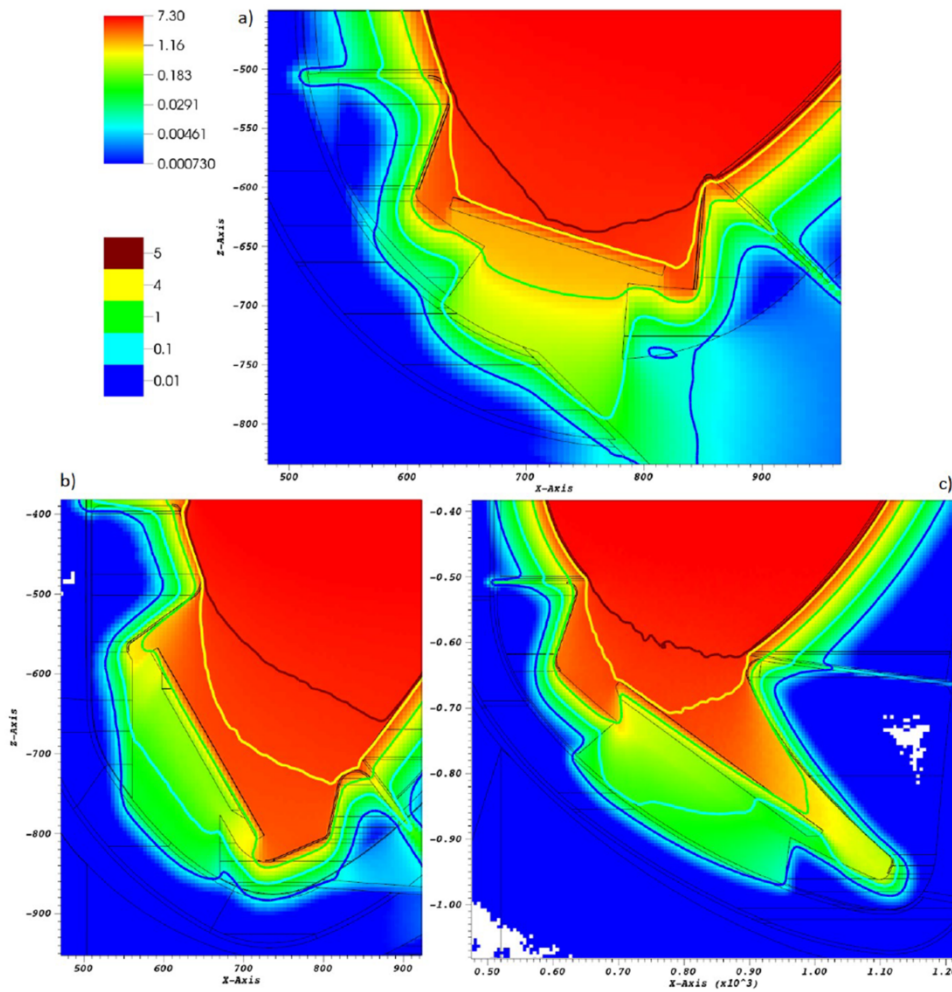
Fig. 7. DPA/FPY in Eurofer for the (a) SN (b) XD and (c) SX configurations at Y=0.

Table 2
Peak DPA/FPY in Eurofer values in each of the divertor configurations.

	SN	SX	XD
Shielding liner	4.14	3.94	3.36
Cassette below IVT	2.85	3.14	0.65
Cassette below OVT	2.99	0.34	1.16

observed in the XD model. This is predominantly the results of an 8 cm gap between the blanket and divertor coupled with bulk transport through the divertor itself. Smaller gaps are also present in the SN and SX models and should be reduced and optimised to mitigate neutron streaming.

- The SX model offers significantly more shielding to the lower port owing to the large cassette body below the outer vertical target and large breeder blanket volume studied in this analysis.

- The poloidal profile of nuclear heating in the TF coils was calculated and determined to exceed the limit of 5×10^{-5} W cm^{-3} on the outboard of the coils in the poloidal sections adjacent to the lower, equatorial and lower ports. The shielding of the SX divertor gives the lowest nuclear heat density in the poloidal segment adjacent to the lower port however for all other segments the limit is exceeded. In the SN and XD models the limit is exceeded for all outboard segments. For all inboard segments, in all configurations, the limit is satisfied.

- Shielding recommendations are made for the cassette body region between the divertor shielding liner and the inner/ outer vertical

targets. The cassette body in each configuration next to the shielding liner is directly exposed to the plasma. The divertor limit of 6 DPA over 1.5 FPY for Eurofer was exceeded only on the shielding liner in the SN configuration however peak values in the region 2–4 DPA/FPY were found for SX and XD which should be reduced to ensure the lifetime of the cassette.

- The pumping port opening gives large responses in the VV shell which sits in the opening. The nuclear heat density in the SN model is equal to 0.3 W cm^{-3} which is at the lower bound of the recommended nuclear heating to the VV, 0.3-0.5 W cm^{-3}. The shielding liner of the XD gives the best shielding of the VV due to its vertical inclination while for the SX a large distribution is seen in the VV because of its length with peak values at the inboard side and values far below the other configurations in outboard below the shielding liner. Such geometric subtleties have a telling effect on the nuclear responses.

- No configuration is shown to exceed the limit of 2.75 DPA over 6 FPY in the VV shell. Peak values are calculated in the SN configuration of 2.38 DPA. As outlined already, careful consideration of the pumping port opening and its impact on the nuclear response is needed.

It is demonstrated that the divertor design has potentially serious ramifications globally for the machine if future evolutions of the design do not mitigate radiation streaming paths or consider shielding solutions. EU DEMO will need to be approved by a regulatory body therefore, as with ITER, demonstration of compliance with nuclear safety will be fundamental prior to the construction or installation of any
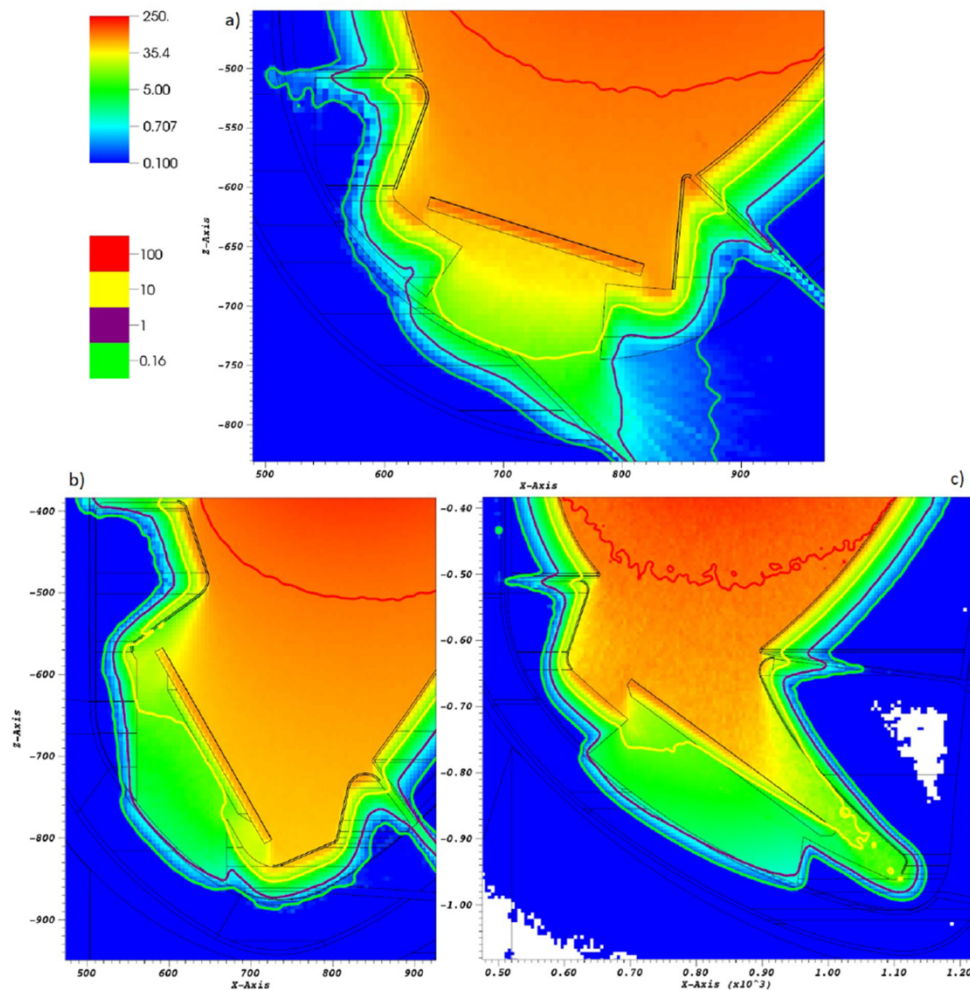
Fig. 8. He production (appm/FPY) in Eurofer for the (a) SN (b) XD and (c) SX configurations at Y=0.

Table 3
Integrated nuclear heating (kW) in PF coil 5 and PF coil 6. Uncertainties are stochastic only.

	SN	SX	XD
PF coil 5	$14.7 \pm 0.16\%$	$0.95 \pm 2.89\%$	$6.54 \pm 0.36\%$
PF coil 6	$6.77 \pm 0.17\%$	$0.16 \pm 6.8\%$	$1.74 \pm 0.41\%$

components.

7. Future work

Future work should include some allocation of void space in the divertor and a lesser degree of homogenisation in the blanket modules and divertor components which are deficiencies in the modelling specific to this analysis. This would give observable differences in responses local to the divertor and the calculated tritium breeding ratio. The CAD model on which the nuclear analysis is performed is produced through optimisation considering plasma physics, the positioning of the blanket and first wall and then the positioning of the coils. Remote maintenance needs must also now be factored in along with, the conclusions presented in this work.

It is not possible to rule out any one of the configurations on the grounds of this analysis - which can be deemed a 'scoping' study. Other divertor configurations not considered in this analysis are being considered as well as hybrid designs. It is crucial that future nuclear analysis is performed in parallel with other engineering and physics analysis for any down selected concept. Through comparing an array of nuclear responses and comparing where possible to design limits, we have demonstrated the importance of performing nuclear analysis at the first design cycle. This is actively demonstrated from the ongoing nuclear analysis of ITER. Shielding corrections at a later stage are not always possible because of for example, space constraints or weight limitations. In this case we are forced to consider revising operations of the machine itself which naturally has significant implications. Efforts must focus on demonstrating both compliance with nuclear limits in parallel with compatibility with the wider constraints of the machine.

CRediT authorship contribution statement

A. Valentine: Conceptualization, Methodology, Software, Validation, Formal analysis, Investigation, Resources, Data curation, Writing - original draft, Visualization, Supervision, Project administration. **N. Fonnesu:** Methodology, Software, Validation, Formal analysis, Investigation, Data curation, Visualization. **B. Bieńkowska:** Methodology, Software, Validation, Formal analysis, Investigation, Data curation, Visualization. **E. Łaszyńska:** Methodology, Software, Validation, Formal analysis, Investigation, Data curation, Visualization. **D. Flammini:** Methodology, Software, Validation, Formal analysis, Investigation, Data curation, Visualization. **R. Villari:** Methodology, Software, Validation, Formal analysis, Investigation, Data curation, Visualization, Writing - review & editing. **G. Mariano:** Methodology, Software, Validation, Formal analysis, Investigation, Data curation, Visualization. **T.**

Declaration of Competing Interest

The authors declare that they have no known competing financial interests or personal relationships that could have appeared to influence the work reported in this paper.

Acknowledgements

References

[1] G. Federici, C. Bachmann, L. Barucca, W. Biel, L. Boccaccini, R. Brown, C. Bustreo, S. Ciattaglia, F. Cismondi, M. Coleman, V. Corato, C. Day, E. Diegele, U. Fischer, T. Franke, C. Gliss, A. Ibarra, R. Kembleton, A. Loving, F. Maviglia, B. Meszaros, G. Pintsuk, N. Taylor, M.Q. Tran, C. Vorpahl, R. Wenninger, J.H. You, DEMO design activity in Europe: progress and updates, Fusion Eng. Des. 136 (April) (2018) 729–741, https://doi.org/10.1016/j.fusengdes.2018.04.001.

[2] R. Dieter-Heuer, A. Aszódi, M. Bautista., R. Hawryluk, J. Vieublé, DEMO G1 Gate Review Panel Report. EFDA_D_2NX, 2020.

[3] F. Militello, R. Ambrosino, T. Body, H. Bufferand, G. Calabro, G. Ciraolo, D. Coster, G.D. Gironimo, P. Fanelli, A. Herrmann, P. Innocente, R. Kembleton, J. Lilburne, T. Lunt, D. Marzullo, S. Merriman, D. Moulton, A.H. Nielsen, J. Omotani, H. Reimerdes, M. Reinhart, P. Ricci, F. Riva, A. Stegmeir, Preliminary analysis of alternative divertors for DEMO, Nucl. Mater. Energy 26 (2021) 1–19.

[4] G. Mazzone, J.H. You, C. Bachmann, U. Bonavolontà, V. Cerri, D. Coccorese, D. Dongiovanni, D. Flammini, P. Frosi, L. Forest, G. Di Gironimo, G. Di Mambro, V. Imbriani, A. Maffucci, D. Marzullo, P.A. Di Maio, M.T. Porfiri, E. Vallone, R. Villari, E. Visca, C. Vorpahl, Eurofusion-DEMO divertor - cassette design and integration, Fusion Eng. Des. 157 (September 2019) (2020), https://doi.org/10.1016/j.fusengdes.2020.111656.

[5] R. Ambrosino, A. Castaldo, S. Ha, V.P. Loschiavo, S. Merriman, H. Reimerdes, Evaluation of feasibility and costs of alternative magnetic divertor configurations for DEMO, Fusion Eng. Des. 146 (April) (2019) 2717–2720, https://doi.org/10.1016/j.fusengdes.2019.04.095.

[6] J. Goorley, Initial MCNP6 Release Overview - MCNP6 Version 1.0. LA-UR-13-22934, 2013.

[7] C.J. Werner, J. Armstrong, F.B. Brown, J.S. Bull, L. Casswell, L.J. Cox, D. Dixon, R. A. Forster, J.T. Goorley, H.G. Hughes, J. Favorite, R. Martz, S.G. Mashnik, M. E. Rising, C. Solomon, A. Sood, J.E. Sweezy, C.J. Werner, A. Zukaitis, C. Anderson, J.S. Elson, J.W. Durkee, R.C. Johns, G.W. McKinney, G.E. McMath, J.S. Hendricks, D.B. Pelowitz, R.E. Prael, T.E. Booth, M.R. James, M.L. Fensin, T.A. Wilcox, B. C. Kiedrowski, MCNP User's Manual Code Version 6.2, Los Alamos National Laboratory, 2017.

[8] Y. Wu, J. Song, H. Zheng, G. Sun, L. Hao, P. Long, L. Hu, CAD-based Monte Carlo program for integrated simulation of nuclear system SuperMC, Ann. Nucl. Energy (2015), https://doi.org/10.1016/j.anucene.2014.08.058.

[9] S.W. Mosher, S.R. Johnson, A.M. Bevill, A.M. Ibrahim, C.R. Daily, T.M. Evans, J. C. Wagner, J.O. Johnson, R.E. Grove, ADVANTG: an automated variance reduction parameter generator, 2015.

[10] NEA, Joint Evaluated Fission and Fusion (JEFF) Nuclear Data Library JEFF-3.3 (2017).

[11] M. White, Further Notes on MCPLIB03/04 and New MCPLIB63/84 Compton Broadening Data For All Versions of MCNP5. LA-UR-12-00018, Los Alamos National Laboratory, 2012.

[12] A. Cufar, DEMO 2017 Baseline Model, HCPB+WCLL. EFDA_D_2NP5TU, 2020.

[13] R. Villari, HCPB MCNP model, Private Commun. (2020).

[14] U. Fischer, C. Bachmann, I. Palermo, P. Pereslavtsev, R. Villari, Neutronics requirements for a DEMO fusion power plant, Fusion Eng. Des. 98-99 (2015) 2134–2137, https://doi.org/10.1016/j.fusengdes.2015.02.029.

[15] M.J. Norgett, M.T. Robinson, I.M. Torrens, A proposed method of calculating displacement dose rates, Nucl. Eng. Des. (1975), https://doi.org/10.1016/0029-5493(75)90035-7.

[16] M.R. Gilbert, S.L. Dudarev, S. Zheng, L.W. Packer, J.C. Sublet, An integrated model for materials in a fusion power plant: transmutation, gas production, and helium embrittlement under neutron irradiation, Nucl. Fusion 52 (8) (2012), https://doi.org/10.1088/0029-5515/52/8/083019.

[17] M.R. Gilbert, S.L. Dudarev, D. Nguyen-Manh, S. Zheng, L.W. Packer, J.C. Sublet, Neutron-induced dpa, transmutations, gas production, and helium embrittlement of fusion materials, J. Nucl. Mater. 442 (1–3 SUPPL.1) (2013) 1–9, https://doi.org/10.1016/j.jnucmat.2013.03.085.

[18] G. Ponti, F. Palombi, D. Abate, F. Ambrosino, G. Aprea, T. Bastianelli, F. Beone, R. Bertini, G. Bracco, M. Caporicci, B. Calosso, M. Chinnici, A. Colavincenzo, A. Cucurullo, P. Dangelo, M. De Rosa, P. De Michele, A. Funel, G. Furini, D. Giammattei, S. Giusepponi, R. Guadagni, G. Guarnieri, A. Italiano, S. Magagnino, A. Mariano, G. Mencuccini, C. Mercuri, S. Migliori, P. Ornelli, S. Pecoraro, A. Perozziello, S. Pierattini, S. Podda, F. Poggi, A. Quintiliani, A. Rocchi, C. Scio, F. Simoni, A. Vita, The role of medium size facilities in the HPC ecosystem: the case of the new CRESCO4 cluster integrated in the ENEAGRID infrastructure. Proceedings of the 2014 International Conference on High Performance Computing and Simulation, HPCS 2014, 2014, https://doi.org/10.1109/HPCSim.2014.6903807.